

**Published in AIChE Journal 2014 Vol. 00, No. 00**

**DOI 10.1002/aic.14546**

**Published online in Wiley Online Library**

***Kinetics of CO<sub>2</sub> Absorption by Aqueous 3-(methylamino)propylamine Solutions: Experimental Results and Modelling***

Juliana G. M.-S. Monteiro<sup>1</sup>, Saddam Hussain<sup>1</sup>, Hammad Majeed<sup>1</sup>, Emmanuel O. Mba<sup>1</sup>, Ardi Hartono<sup>1</sup>, Hanna Knuutila<sup>1</sup>, Hallvard F. Svendsen<sup>1\*</sup>

<sup>1</sup>Department of Chemical Engineering, Norwegian University of Science and Technology, N-7491 Trondheim, Norway

\* Corresponding author: hallvard.svendsen@chemeng.ntnu.no

Phone: 73594100

Address: Kjemi IV\*402 Sem Sælands vei 6

Department of Chemical Engineering

Norwegian University of Science and Technology

7491 Trondheim

**Abstract**

This work presents experimental data and a model for the initial kinetics of CO<sub>2</sub> into 3-(methylamino)propylamine (MAPA) solutions. MAPA has been tested as an activator for tertiary amines with encouraging results. The measurements were performed in a string of discs contactor and, since no initial kinetics data is available in literature, additional measurements were carried out in a wetted wall column. The obtained overall mass transfer coefficients from both apparatuses are in reasonable agreement. To obtain values for the observed kinetic constant,  $k_{obs}$ , the experimental results were interpreted using a two-film mass-transfer model and invoking the pseudo first order assumption. Needed experimental values for density, viscosity and Henry's law coefficient for CO<sub>2</sub> were measured and are given. The results indicate that MAPA is almost twice as fast as PZ, 8 times faster than AEEA, and 15 times faster than MEA, when comparing unloaded 1M solutions at 25°C. The observed kinetic constant

was modelled using the direct mechanism. The final expression for  $k_{obs}$  can be applied for any concentration and temperature within the experimental data range, and, together with the presented physical data, comprises a complete model for calculating absorption fluxes.

## Introduction

An ideal amine for CO<sub>2</sub> absorption should combine fast kinetics, reasonable heat of absorption, and high equilibrium temperature sensitivity, all potentially reducing the regeneration energy requirement and absorber size. Typically the aim is a solvent that gives an optimal trade-off between fast kinetics and low energy requirements. One possibility is blending carbamate formers, primary or secondary amines (activators), with tertiary or sterically hindered amines which would preferentially give bicarbonate formation and thus possibly lower the energy demand for regeneration.

This work presents new experimental data and a model for the initial kinetics of CO<sub>2</sub> into 3-(methylamino)propylamine (MAPA) solutions. MAPA is a diamine with one primary and one secondary group, and it has been shown that the CO<sub>2</sub> absorption rates into 8m MAPA at low CO<sub>2</sub> partial pressures are higher than for 8m MEA<sup>1</sup>. Screening tests performed by Brúder, Svendsen<sup>2</sup> at 40°C and below 10kPa CO<sub>2</sub> partial pressure indicate that the initial absorption rate of 5M MAPA is higher than that of 5M MEA, and this difference increases with loading. Additionally, loadings as high as 5 mol CO<sub>2</sub>/kg of solution were obtained<sup>2</sup>. MAPA has been tested as an activator for dimethyl-monoethanolamine<sup>3</sup>, N,N-diethylethanolamine<sup>4</sup>, 2-amino-2-methyl-1-propanol<sup>5</sup>, triethylamine and N,N-dimethylbutylamine<sup>6</sup> with encouraging results.

## Measurements

### Chemicals

MAPA (CAS number: 6291-84-5) was obtained from Sigma Aldrich with purity  $\geq 98\%$ , while the gases were supplied by AGA Gas GmbH and Yara with purity  $\geq 99,99$  mol% for CO<sub>2</sub> and  $\geq 99,999$  mol% for N<sub>2</sub>. MAPA solutions were prepared by weighing in and mixing the solvent with DI water at room temperature.

## Kinetics

A string of discs contactor was used for studying the reactive absorption of CO<sub>2</sub> into liquid MAPA solutions. This type of apparatus was first described by Stephens, Morris <sup>7</sup> as a suitable apparatus for determining absorption coefficients experimentally. The string of discs column (SDC) used in this work has 43 discs of 4mm thickness and 1.5 cm diameter, leading to a column length of 64.5 cm and a total mass transfer area of 0.0219 m<sup>2</sup>. The apparatus, previously described by Ma'mun, Dindore, Svendsen <sup>8</sup>, Knuutila, Svendsen, Juliussen <sup>9</sup> and Hartono, Svendsen <sup>10</sup>, among others, promotes the contact of a gas stream (a mixture of N<sub>2</sub> and CO<sub>2</sub>) and a liquid solution in counter-current mode. Figure 1 shows the experimental set-up of the SDC apparatus.

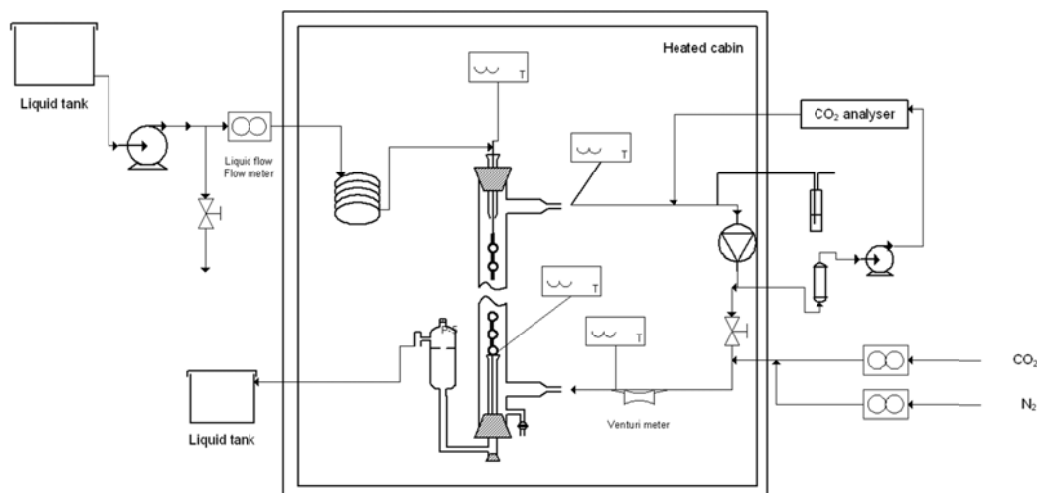


**Figure 1 – Experimental set-up of the SDC apparatus <sup>9</sup>**

The inlet flow rates of N<sub>2</sub> and CO<sub>2</sub> were set using mass flow controllers with uncertainty less than 1% of measured flow, while the CO<sub>2</sub> composition in the outlet gas was determined by an IR CO<sub>2</sub> analyser. The analyser was calibrated every day, before the measurements were made, and the accuracy in the readings were 0.01%. The gas was circulated in the system with a flow rate of approximately 3 m<sup>3</sup>/h, while the liquid flow was once through and the rate was kept constant at approximately 50 ml/min. The operation was carried out at ambient pressure and pressure indicators for the gas inlet and outlet streams determined the pressure drop along the column.

The column is enclosed in an insulated heating chamber and the experiments were performed in the temperature range 25°C to 62°C. An experimental point was considered stable when the temperatures of the gas and liquid streams at the top and bottom of the column, as well as the gas composition, showed constant values for at least 5 minutes. The calculations considered the averages of 2 minutes online readings, and the standard deviations in the measurements within this period were used for uncertainty evaluations.

The experiments were conducted for unloaded aqueous solutions of MAPA at the following concentrations: 1M (9wt%), 2M (18wt%), 3M (27wt%), 4M (36wt%) and 5M (45wt%). The end solutions were analysed for total alkalinity and CO<sub>2</sub> content. All analyses indicated no measurable variation in the amine content of the solutions. The final loadings were always smaller than 0.01 mol CO<sub>2</sub>/mol MAPA.

Because there's no data available in the literature for the kinetics of unloaded MAPA solutions, extra measurements for the 2M MAPA solution were performed in a wetted wall column. The apparatus and the experimental procedures are described in detail by Luo, Hartono, Svendsen<sup>11</sup>, who showed that the measurements performed in the two apparatuses are consistent.

#### Physical properties

In order to interpret the results obtained in the SDC experiments, it was necessary to determine the following physical properties of the solutions: density, viscosity, Henry's constant and diffusivity of CO<sub>2</sub>. The two first properties were measured directly. Henry's law constant of CO<sub>2</sub> was calculated from measurements of Henry's constant of N<sub>2</sub>O in the solution by using the N<sub>2</sub>O analogy<sup>12</sup>. The diffusivity of CO<sub>2</sub> in the solution was estimated using the correlations given by Versteeg, Van Dijck, Van Swaaij<sup>13</sup>.

The viscosities of the MAPA solutions were determined using an Anton Paar Rheometer Physica MCR 100, with the DG 26.7 measuring system and the TEK 150P-C measuring cell. Series of repeated measurements indicated that the uncertainty of the viscosity measurements is around ± 2% for the viscometer used in this work<sup>14</sup>. The experimental results from 20 to 80°C are given in Table 1.

The densities were measured using an Anton Paar Stabinger Density Meter DMA 4500. Nominal repeatability is of 10<sup>-5</sup> g/cm<sup>3</sup> for density and 0.01°C for temperature. Series of repeated measurements indicated that the uncertainty of the density measurements was ± 3\*10<sup>-5</sup> g/cm<sup>3</sup><sup>15</sup>. The experimental results

from 20 to 70°C are given in Table 2. These results are in good agreement with those obtained by Pinto, Monteiro, Johnsen, Svendsen, Knuutila<sup>15</sup>.

The N<sub>2</sub>O solubility apparatus used and the calculation procedure for determining Henry's constant of N<sub>2</sub>O are described in detail by Knuutila, Juliussen, Svendsen<sup>16</sup>. The measurements were carried out from 25 to 65°C. The results are given in **Table 3**. The uncertainty of the measured N<sub>2</sub>O solubilities is estimated to be ± 7.5%.

**Table 1 – Viscosity Data for MAPA Solutions, mPa.s**

T (°C)	1M	2M	3M	4M	5M
20	1.598	2.527	4.353	7.655	13.057
25	1.397	2.135	3.566	6.037	9.944
30	1.234	1.834	2.977	4.875	7.729
40	0.981	1.402	2.164	3.332	4.974
50	0.808	1.120	1.649	2.416	3.364
60	0.702	0.921	1.311	1.833	2.362
70	0.601	0.778	1.072	1.437	1.774
80	0.503	0.647	0.870	1.159	1.361

**Table 2 – Density Data for MAPA Solutions, g.cm<sup>-3</sup>**

T (°C)	1M	2M	3M	4M	5M
20	0.99221	0.98854	0.98647	0.98438	0.97873
30	0.98914	0.98445	0.98098	0.97742	0.97077
40	0.98522	0.97963	0.97499	0.97018	0.96257
50	0.98047	0.97428	0.96854	0.96269	0.95425
60	0.97541	0.96836	0.96176	0.95496	0.94585
70	0.96966	0.96198	0.95458	0.947	0.93718

**Table 3 – Henry's Law Constant for N<sub>2</sub>O in MAPA Solutions, Pa.m<sup>3</sup>.mol<sup>-1</sup>**

T (°C)	1M	2M	3M	4M	5M
25	4316	4803	5674	6584	6869
35	5533	5957	6625	7354	7348
45	6822	7200	7629	8030	7650
45	6790	7131	-	8031	-

55	8345	8467	8599	8640	8003
55	-	-	8529	-	-
65	10145	10090	9719	9311	8508

Calculation of the pseudo first order kinetic constant

From the performed experiments in both the SDC and the WWC, the CO<sub>2</sub> absorption flux is determined by a mass balance (equation 1). The inlet CO<sub>2</sub> and N<sub>2</sub> fluxes were measured directly by mass flow. A side stream of the circulating gas is analysed online for CO<sub>2</sub> using an IR analyser. Prior to the analysis, the gas is cooled down to 20°C to avoid water condensation in the analyser. The condensate is separated and the dry gas passes to the analyser (see Figure 1). The CO<sub>2</sub> outlet flux can be calculated from Eq. 2. In this equation,  $y_{CO_2,out}$  is the mol fraction of the dried gas, as read from the analyser and  $N_{N_2,out} = N_{N_2,in}$  is the small but constant flow of inert through the apparatus.

$$N_{CO_2} = N_{CO_2,in} - N_{CO_2,out} = N_{N_2,in} (y_{CO_2,in} - y_{CO_2,out}) \quad \mathbf{1}$$

$$N_{CO_2,out} = N_{N_2,in} \frac{y_{CO_2,out}}{1 - y_{CO_2,out}} \quad \mathbf{2}$$

The overall mass transfer coefficient can be calculated as the ratio between the CO<sub>2</sub> absorption flux and the driving force (equation 3). Since the experiments reported in this work comprise only unloaded solutions, the logarithmic mean of the CO<sub>2</sub> partial pressure difference in the inlet and outlet streams was calculated using equation 4.

$$K_{ov} = \frac{N_{CO_2}}{\Delta p_{CO_2}^{LM}} \quad \mathbf{3}$$

$$\Delta p_{CO_2}^{LM} = \frac{P_{CO_2,out} - P_{CO_2,in}}{\ln\left(\frac{P_{CO_2,out}}{P_{CO_2,in}}\right)} \cong \frac{P_{CO_2,out} + P_{CO_2,in}}{2} \quad \mathbf{4}$$

By applying the two-film theory <sup>17</sup>, the overall mass transfer coefficient can be split into a gas- and a liquid-side mass transfer coefficient, as shown in equation 5. Given that the reaction takes place in the pseudo-first order regime ( $Ha \geq 3$  and  $E \ll E_\infty$ ), the enhancement factor is equal to the Hatta number and given by equation 6 <sup>17</sup>. Hence, the pseudo first order kinetic constant can be calculated from equations 5 to 7.

$$K_{ov} = \frac{1}{\frac{1}{k_G} + \frac{H_{CO_2}}{Ek_L^0}} = \frac{1}{\frac{1}{k_G} + \frac{H_{CO_2}}{k_L}} \quad 5$$

$$E = Ha = \frac{\sqrt{k_{obs} D_{CO_2}}}{k_L^0} \quad 6$$

$$k_{obs} = \frac{H_{CO_2}^2}{\left(\frac{1}{K_{ov}} - \frac{1}{k_G}\right)^2 D_{CO_2}} \quad 7$$

The gas film mass transfer coefficient,  $k_G$ , and the liquid film physical mass transfer coefficient,  $k_L^0$ , are dependent on the gas and liquid flow properties, respectively, as well as the apparatus geometry, and were calculated using the correlations given by Ma'mun, Dindore, Svendsen <sup>8</sup> for this SDC.

#### Uncertainty Evaluation

The measurements were saved in a log file every 10 seconds. When the experiment reached a stable condition, a point was taken by averaging the logged values over 2 minutes (i.e., considering 12 log entries). This should be a large enough number to provide a reliable standard deviation <sup>18</sup>. Hence, if  $x$  is a measured quantity, the value used in the calculations was its average ( $\bar{x}$ , given by equation 8), and the measurement uncertainty,  $u_x$ , was given by its standard deviation (equation 9), as the uncertainties are considered to have a normal distribution.

$$\bar{x} = \frac{1}{12} \sum_{i=1}^{12} x_i \quad \mathbf{8}$$

$$u_x = \sqrt{\frac{1}{11} \sum_{i=1}^{12} (x_i - \bar{x})^2} \quad \mathbf{9}$$

The propagation of these uncertainties will reflect on the uncertainty of the calculated variables, such as  $K_{ov}$  and  $k_{obs}$ . Given a generic calculated variable, as defined in equation 10, the propagation equation 11 is used to assess its uncertainty <sup>18</sup>.

$$f = f(a_1, a_2, \dots, a_n) \quad \mathbf{10}$$

$$u_f = \sqrt{\sum_{k=1}^n \left( \frac{\delta f}{\delta a_k} \right)^2 u_{a_k}^2} \quad \mathbf{11}$$

#### Modelling of the pseudo first order kinetic constant

Many reactions take place when CO<sub>2</sub> is absorbed by aqueous amine solutions. The direct reaction of CO<sub>2</sub> with water, reaction 12, is negligible at high pH <sup>9</sup> and was therefore disregarded in this work. Additionally, the reaction of CO<sub>2</sub> with hydroxyl ion, reaction 13, was found to be negligible (in all tested cases its contribution to the overall rate was less than 0.1%).

This indicates that the CO<sub>2</sub> absorption by unloaded aqueous MAPA solutions takes place mainly through the reactions of carbamate formation. The formation of MAPA carbamates can occur either on the primary or the secondary amine functionalities, and this is indicated by the subscripts  $p$  and  $s$  on the carbamate species. A simplified representation of the carbamate formation reactions is given in reactions 14 and 15. Since all the experiments in this work were performed on initially unloaded amine, the possible formation of a di-carbamate could safely be disregarded as shown by Ciftja, Hartono, Svendsen <sup>19</sup>. The structures of the two different MAPA carbamates are given in Figure 2.



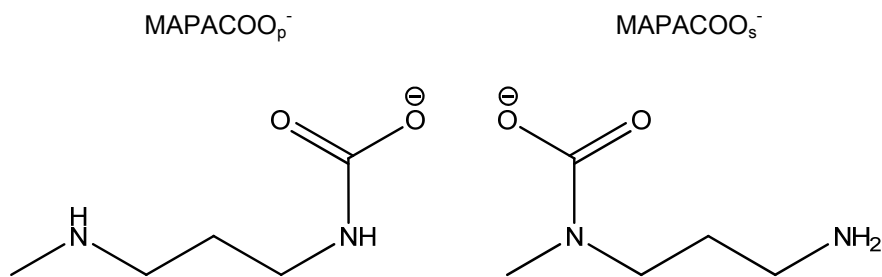


**Figure 2 – MAPA carbamates**

The observed reaction rate is actually the sum of the rate of formation of the two carbamate species. There is no way of differentiating the rate of formation of primary from that of secondary carbamates from the experiments performed in this work. The results of Ciftja, Hartono, Svendsen<sup>19</sup> indicate that already at low loadings both carbamates are present at equilibrium, and the concentration of the primary carbamate is about 3 to 4 times that of the secondary. As it would be very uncertain to apply the same ratio for initial kinetics, we have decided to consider the sum of the carbamate formation rates in our analysis.

The carbamate reactions require the presence of a base component. As mentioned earlier, the loading values throughout the experiments performed in this work were very low, practically negligible. Therefore only MAPA and water were considered as relevant bases. Other basic species such as the formed mono-carbamates are present only in very low concentrations.

There are two traditional mechanisms proposed in the literature for explaining the reaction between  $CO_2$  and primary or secondary amines. The first mechanism suggests a two-step reaction with the formation of a zwitterion as intermediate<sup>20</sup>. The second mechanism proposes a direct reaction where the nitrogen

atom in the amine bonds with the carbon atom in CO<sub>2</sub> while a proton is simultaneously transferred from the amino nitrogen to an already complexated base, water or amine <sup>21</sup>.

da Silva, Svendsen <sup>22</sup> performed ab initio calculations using a continuum model and concluded that the direct mechanism is the most likely. Shim, Kim, Jhon, Kim, Cho <sup>23</sup> performed a similar study, considering a polarizable continuum, and achieved the same result. In the study presented by Arstad, Blom, Swang <sup>24</sup>, water molecules are explicitly included in the molecular model. The authors also conclude that a mechanism very similar to that proposed by Crooks, Donnellan <sup>21</sup> seems to take place and suggest that the transition state may be of zwitterionic nature. Based on these works, we have chosen to model the reaction according to the direct mechanism. Hence, the total rate of carbamates formation is given by equation 16. This expression can also be arrived at by means of the zwitterion mechanism, but in that case it would be necessary to assume that the rate of deprotonation of the zwitterion is the rate determining step, which seems unlikely.

$$-r_{CO_2} = \{k_{MAPA}c_{MAPA} + k_{H_2O}c_{H_2O}\}c_{MAPA}c_{CO_2} \quad \mathbf{16}$$

The pseudo first order kinetic constant ( $k_{obs}$ ) is modelled as in equation 17. The kinetic constants in the model were assessed using the Arrhenius deterministic relation, i.e., they were unfolded into one pre-exponential (or frequency) factor, ( $a_i$ ), and one energy factor, ( $b_i$ ), as in equation 18.

$$k_{obs} = \{k_{MAPA}c_{MAPA} + k_{H_2O}c_{H_2O}\}c_{MAPA} \quad \mathbf{17}$$

$$k_{obs} = \left\{ a_{MAPA} \exp\left(\frac{b_{MAPA}}{T}\right) c_{MAPA} + a_{H_2O} \exp\left(\frac{b_{H_2O}}{T}\right) c_{H_2O} \right\} c_{MAPA} \quad \mathbf{18}$$

The pre-exponential factor is connected to the frequency of collisions between reactants, while the energy factor is related to the activation energy through equation 19 <sup>25</sup>.

$$b_i = \frac{-E_{act,i}}{R}$$

Taking these physical meanings into consideration, the frequency factors may be dependent on the solution concentration and on the temperature. The temperature dependency of the frequency factor is actually predicted by both Collision and Transition State theories, but its influence is normally very small when compared to the exponential term<sup>26</sup>.

The energy factor is normally not considered to be a function of concentration nor temperature, since the activation energy depends only on the energy level of the reactants and that of the transition state complex. Hence, in this work, the frequency factor is considered a function of the concentration only, while the energy factor is independent both of concentration and temperature.

The physical meaning attributed to the frequency and the energy factors, on the other hand, is only valid when elementary reactions are taken into consideration (i.e., no intermediates are formed).

In order to understand the mechanism of CO<sub>2</sub> absorption into aqueous MAPA solutions, fundamental knowledge of the liquid structure, not obtainable from macroscopic kinetic studies, is needed. Molecular modelling studies on the CO<sub>2</sub> absorption in aqueous MEA solutions are available in literature<sup>22-24,27-29</sup>. Because studies with different modelling premises may come to different conclusions regarding the stability of conformers, caution should be taken when evaluating the results. For instance, Han, Zhou, Wu, Tempel, Cheng<sup>28</sup> indicate that, although MEA molecules may form ring structures (due to internal hydrogen bonding), the chain configuration is the most stable when water molecules are explicitly included in the model.

Amongst the different studies, there are also differences regarding which species take part in the carbamate formation reaction. While some studies<sup>27-29</sup> indicate that only MEA molecules act as proton receivers, the simulations performed by Arstad, Blom, Swang<sup>24</sup> show the possibilities of both MEA and water acting as proton receivers and show that the activation energy for water is considerably higher than for MEA.

da Silva, Kuznetsova, Kvamme, Merz<sup>27</sup> conclude that there is a low degree of interaction between the amine functionalities of different MEA molecules (in a 30wt% solution), and suggest that the event of

having a CO<sub>2</sub> molecule, a reacting MEA molecule and a second MEA molecule is relatively rare. Because the MEA carbamate formation is relatively fast, this result may suggest that another molecule – water – will act as a base.

Gupta, da Silva, Svendsen<sup>30</sup> actually address the formation of MAPA carbamates using an explicit solvation shell model. The authors simulate clusters of MAPA (or MAPA carbamate) and five water molecules and show that while the chain MAPA conformer is the most stable structure in unloaded aqueous solutions, due to strong interactions between the nitrogen atoms in MAPA and water molecules, the carbamate is more stable in a cyclic form, as shown in Figure 3. However, the mechanism of formation of the carbamate is not discussed.

MAPACOO<sub>p</sub><sup>-</sup>

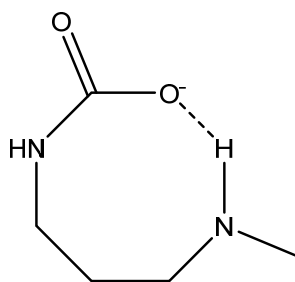


**Figure 3 – Cyclic MAPA carbamate. The dotted line represents a hydrogen bond.**

None of the studies mentioned in this section provide a study on the effects of solution concentration and temperature on conformers stability. Such effects could directly influence the kinetics of carbamate formation.

## Results and Discussion

### Pseudo first order kinetic constant

The experimental data, physical properties and calculation results for the transport and the pseudo-first order kinetic constants are presented in Appendix 1 for the solutions of MAPA with concentrations varying from 1M to 5M. It can be seen that the experiments show good reproducibility and the results obtained in

2011 do not show any systematic deviation from those obtained in 2013. Moreover, the repeatability is also good.

The string of discs column and the gas lines are placed inside an insulated heating chamber and the liquid solution flows through a coil before reaching the column inlet. Additionally the gas stream is saturated prior to the column to avoid evaporation from the liquid phase. However, these measures did not guarantee equal gas and liquid inlet and outlet temperatures.

Typically, the liquid inlet and outlet temperatures departed 2°C from each other, but  $\Delta T$  up to 4.6°C was observed in the low concentration, high temperature range. Normally the liquid inlet temperatures were lower than the outlet temperatures and the difference can be a consequence of the heat of reaction. The gas inlet temperatures were normally 2°C higher than the outlet, and up to 4°C higher than the liquid inlet. The higher gas temperatures can be due to the heat generated by the gas fan upstream the gas inlet temperature measurement.

Therefore, the temperatures presented in Appendix 1 are the averages of the liquid inlet and outlet readings. This is believed to give the best representation of the temperature at which the CO<sub>2</sub> absorption takes place in each experiment.

The physical properties presented in Appendix 1 are calculated for the actual experimental solution concentration and temperature based on the values given in this work by bilinear interpolation.

The calculated overall mass transfer coefficients are shown in Figure 4. As previously observed for the CO<sub>2</sub> absorption by other amines at approximately the same temperature range<sup>11,31,32</sup>, they increase with increasing temperature and also show a strong dependency on the solution concentration.

Because the absorption reaction is exothermic (and therefore less favoured at higher temperatures), and since the gas solubility decreases with temperature, the observed increase of the overall mass transfer coefficient with temperature can only be due to the temperature effect on the reaction kinetics.

Moreover, Kim<sup>33</sup> has shown that the heat of absorption of CO<sub>2</sub> in 8wt% MAPA (~1M) increases from around -85kJ/mol at 40°C to -90kJ/mol at 80°C in the low loading region. Hence, at the experimental range of the kinetics experiments (25°C to 60°C), this effect is nearly negligible.

There is a reasonably good agreement between the data obtained in the SDC (triangles) and in the WWC (crosses) for the 2M MAPA solution. However, because no uncertainty analysis was performed for the data obtained in the WWC, those were not included in the parameter fitting procedure.

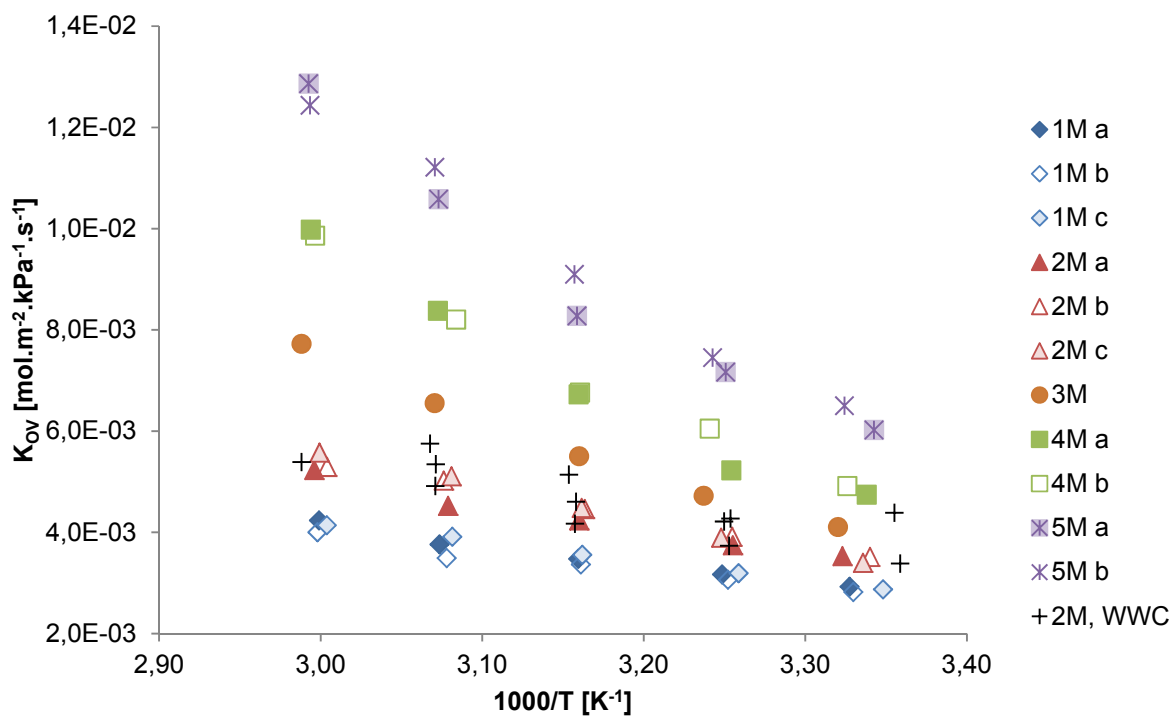


**Figure 4 – Calculated values for  $K_{ov}$  as a function of temperature.**

The pseudo first order kinetic constant ( $k_{obs}$ ) shows a reasonably linear behaviour in the Arrhenius diagram (Figure 5), especially for concentrations up to 3M. Changes in the slope can be either an indication of a shift in the controlling reaction mechanism<sup>34</sup> or a consequence of experimental errors. If the data are believed to be correct, as the good agreement between parallel measurements suggests, then, from equation 17, the changes in the slopes are results of a physical change in the roles of MAPA and water as proton receivers. As mentioned earlier, the kinetic data represent the sum of carbamate formation both on the primary and secondary amine groups. These cannot be distinguished, and a shift from e.g. predominantly a primary carbamate formation to more secondary carbamate formation, may explain the change in slope.

The calculated uncertainties in the  $K_{ov}$  measurements, as defined in 3.1, were in this work found to be around 1%. From Figure 5 it can be seen that the actual variability in the data is greater than 1%, and the practical repeatability of  $K_{ov}$  is about 5%. This means that error sources that are not computed, such as random experimental errors, are the main contributors to the observed variability in  $K_{ov}$ .

Since density and viscosity data are reasonably accurate, and given that the dependency of the observed first order kinetic constant to these properties is not high, these measurements do not contribute significantly to the uncertainty in  $k_{obs}$ . Apart from the uncertainty in  $K_{ov}$ , another major source of uncertainty in the  $k_{obs}$  calculations comes from the solubility data. Given that the Henry constant's uncertainty could be estimated to  $\pm 7.5\%$ , it follows that the uncertainty in  $k_{obs}$  will be at least 15% (since  $k_{obs}$  is proportional to the square of the Henry's constant).

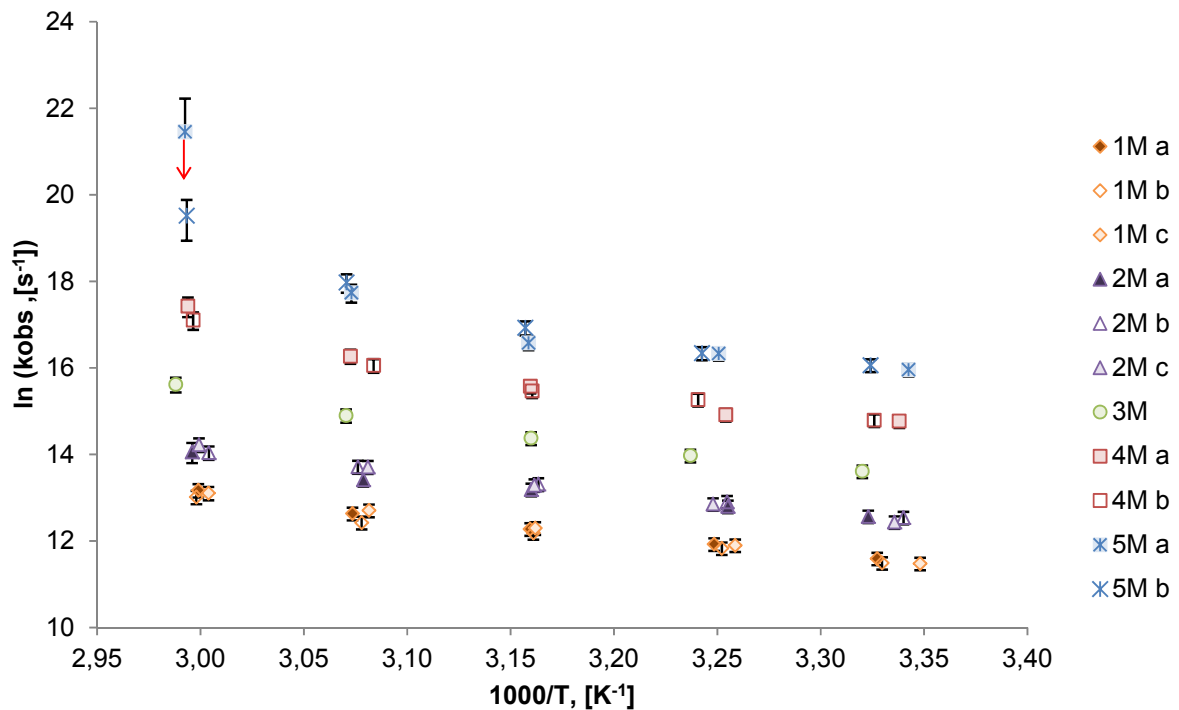


**Figure 5 – Arrhenius plot of  $k_{obs}$ . The uncertainty for the 5M a run at 61°C was greater than 100%.**

**Due to the logarithmic plot, the negative error bar cannot be properly represented. A red arrow is included to graphically indicate this.**

The experimental procedure used is based on steady state stable levels of CO<sub>2</sub> in the gas circulation loop. The experiments performed at high MAPA concentrations and temperatures show significantly more unstable readings for the gas phase CO<sub>2</sub> concentration than for other conditions. For that reason, the points for 4M (runs a and b) at 61°C and 5M (runs a and b) at 52°C have uncertainties of at least 20%; while the points for 5M at 61°C have uncertainties of at least 110% (run a) and 44% (run b). The value obtained in “run a” for 5M MAPA solution at 61°C is therefore not reliable at all, and was only included in this work to illustrate the influence of the fluctuations in the readings on the obtained results, as well as to stress the importance of evaluating the data uncertainties and considering such information when modelling.

In the uncertainty analysis some simplifying assumptions had to be made. For instance, the correlation for determining  $k_G$  was considered to be exact, as well as the relationship between MAPA diffusivity in the solution and the solution viscosity. However, the obtained values for the uncertainties are considered to be a good approximation of the real values, and are therefore taken into consideration in the parameter regression.

#### Parameter regression

The expressions obtained by applying the direct mechanism to describe carbamate formation are summations of exponentials, as in equation 12. Applying a logarithmic transformation to this form of equations would result in polynomials in  $1/T$  with an order determined by the number of terms in the summation. Therefore, the logarithmic transformation of equation 18 would result in a second order polynomial. However, if only one base is considered, the transformation results is a linear function in  $1/T$ , and the parameters can be obtained by linear regression.



Literature provides an interesting debate on the regression of the Arrhenius equation parameters. While Brauner, Shacham <sup>35</sup>, Curl <sup>36</sup> and Sundberg <sup>37</sup> defend the linearization of the equation, Schwaab, Pinto <sup>26</sup>, Chen, Aris <sup>38</sup>, and Klicka, Kubáček <sup>39</sup> argue against it. According to Schwaab, Pinto <sup>26</sup>, the logarithmic transformation of the Arrhenius equation is better avoided because it is otherwise difficult to keep the error structure of the experimental observations.

To avoid controversial and cumbersome statistical treatment of the kinetic constants and respective uncertainties, in this work we chose to follow the approach of Schwaab, Pinto <sup>26</sup> and inserted the Arrhenius equation into the kinetic rate expressions, equation 18, and used the heuristic particle swarm optimization (PSO) algorithm <sup>40</sup> to perform a nonlinear regression and provide both the parameter estimates and a statistical evaluation of the joint confidence regions. Schwaab, Biscaia, Monteiro, Pinto <sup>41</sup> show that the confidence regions of kinetic constants can be very complex, showing non-convexity and being constituted by disconnected regions.

The PSO algorithm does not require initial guesses for the model parameters and does not use derivatives. It was implemented using the local best topology and the tuned PSO parameter values presented by Poli, Kennedy, Blackwell <sup>42</sup>. Details of the implementation of the PSO method are given elsewhere <sup>43</sup>.

The parameter regression problem is formulated as a minimization of the squared difference between the experimental and the modelled value of the pseudo first order kinetic constant, weighed using the estimated uncertainties. The variables transformations presented in equations 20 and 21 were used in order to avoid numeric precision issues connected to very high values of the pre-exponential terms. The final formulation is presented in equation 22.

$$\alpha_{MAPA} = \ln a_{MAPA} \quad \mathbf{20}$$

$$\alpha_{H_2O} = \ln a_{H_2O} \quad \mathbf{21}$$

$$F_{obj}(j) = \sum_{i=1}^{NP(j)} \frac{\left( k_{obs}(i,j) - \left\{ \exp\left(\alpha_{MAPA} + \frac{b_{MAPA}}{T}\right) c_{MAPA}(i,j) + \exp\left(\alpha_{H_2O} + \frac{b_{H_2O}}{T}\right) c_{H_2O}(i,j) \right\} c_{MAPA}(i,j) \right)^2}{u_{kobs}^2(i,j)} \quad 22$$

The optimization was performed in two steps. Initially, 12 parameters were fitted using all the experimental data available: 2 energy parameters,  $b_{MAPA}$  and  $b_{H_2O}$ , which are the same regardless of the solution concentration, and 10 pre-exponential parameters,  $\alpha_{MAPA}$  and  $\alpha_{H_2O}$ , (i.e., 2 per solution concentration). In the second step, the optimized energy parameters were kept constant and 5 optimizations were carried out, one for each concentration. This reduces the problem to be solved, since only two parameters are fitted and the number of experimental points available varies from 5 to 15 per solution concentration.

The optimization results are presented in Table 4. Using equation 19, the activation energies obtained are 39 kJ/mol for MAPA and 182 kJ/mol for water respectively. The value obtained for MAPA is similar to those obtained by Ma'mun, Dindore, Svendsen<sup>8</sup> and Bishnoi, Rochelle<sup>32</sup> for AEEA and PZ, respectively. The value obtained for water is very high, and although it could be argued that Arstad, Blom, Swang<sup>24</sup> predicts high activation energy for the MEA carbamate formation when water is the proton receiver, this result should be interpreted with care since such a high number may be a mathematical artefact to allow the proposed model to fit the experimental data. The model adopted in this work is relatively simple and does not account for possible changes in the solution structure with temperature and concentration. One may speculate that at low temperature and high MAPA concentration, the ring structure predicted by Gupta, da Silva, Svendsen<sup>30</sup> is stable, resulting in the dominating effect of MAPA as base (it is assumed that while one nitrogen of the MAPA molecule reacts with  $CO_2$ , the second nitrogen is close enough to act as a base, forming a zwitterion as a transition species). At low MAPA concentrations and higher temperatures, the ring structure may become less stable leading to a stronger effect of water as base. Thus, relatively speaking, the effect of water could increase significantly, and this may at least partly explain the high apparent activation energy obtained. However, directly inferring the mechanistic behaviour from the results presented herein may be stretching the obtained model beyond its possibilities.

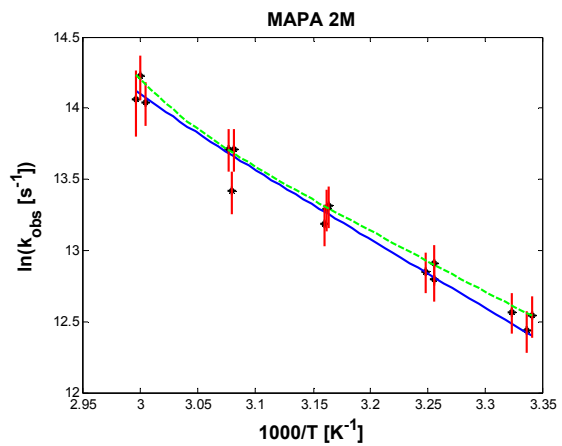
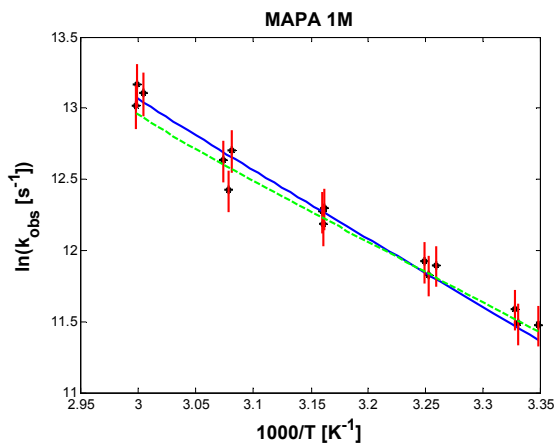
The goodness of the fit can be evaluated from the average relative deviation, defined in equation 23, as well as from the plots presented in Figure 6. The somewhat high ARD for MAPA 5M is due to the point at 60°C, run a. Since the uncertainties are taken into consideration in the objective function, the obtained minimum value is comparable to that obtained for 1M.

$$ARD = \frac{1}{NP} \sum_{i=1}^{NP} \frac{|k_{obs}^{exp} - k_{obs}^{mod}|}{k_{obs}^{exp}}$$

23

**Table 4 – Optimization Results**

MAPA concentration	$F_{obj}$	ARD %	$\alpha_{MAPA}$	$a_{MAPA}$	$b_{MAPA}$	$\alpha_{H_2O}$	$a_{H_2O}$	$b_{H_2O}$
1M	7,8	8,4	13,58	793731	-4792	58,87	3,69E+25	-22365
2M	6,8	7,3	13,19	534774		60,12	1,28E+26	
3M	0,02	0,8	13,47	710838		62,92	2,12E+27	
4M	4,3	9,3	14,02	1229355		65,00	1,69E+28	
5M	10,6	23,5	14,80	2674572		66,98	1,23E+29	



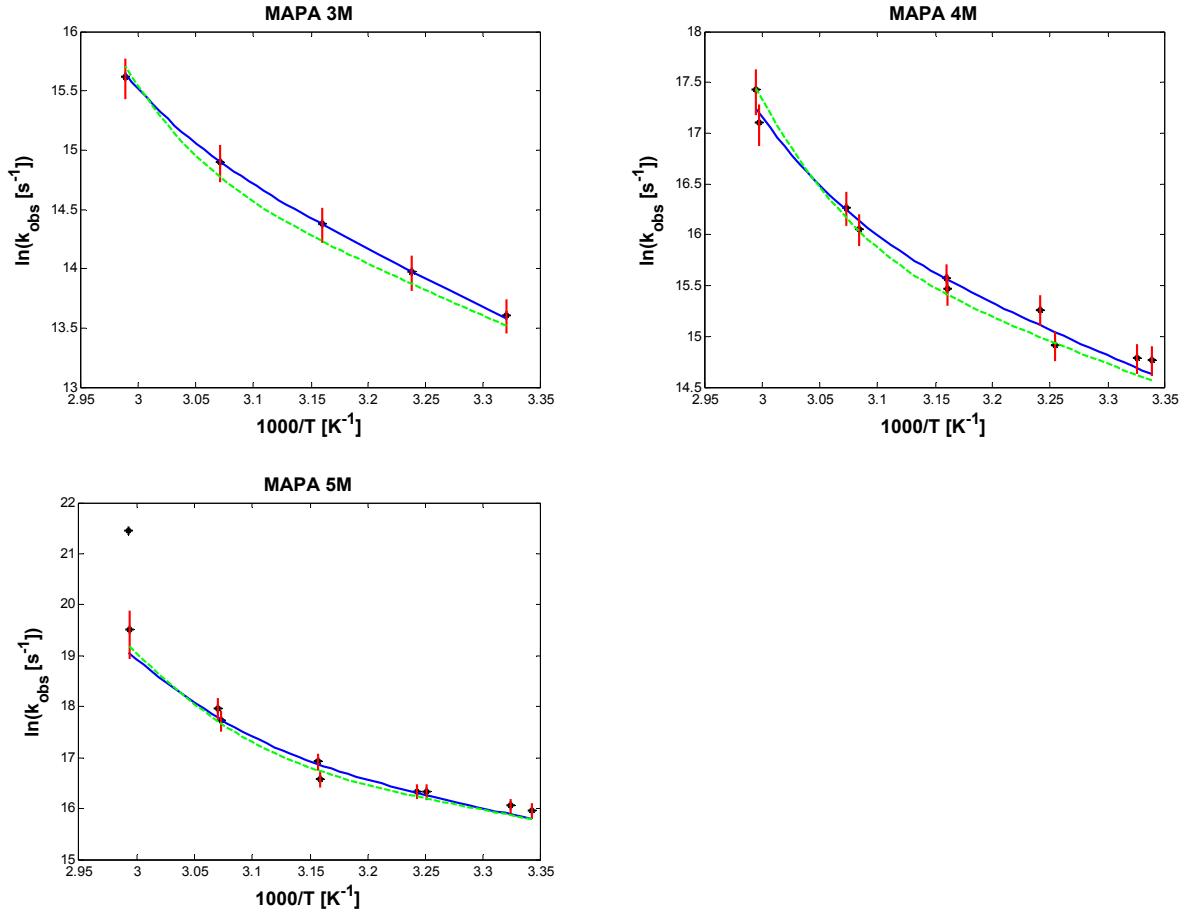


**Figure 6 – Arrhenius plots showing the optimization results. Black points: experimental points presented in this work. Red vertical lines: error bars. Blue lines: fitted model using equation 22. Green lines: fitted models using equation 27.**

The obtained model can explain the observed data very well. However, the estimated value for  $b_{H_2O}$  leads to extremely low values for the exponential function, causing the estimated values for  $a_{H_2O}$  to be extremely high. The multiplication of the two factors give  $k_{H_2O}$  with magnitudes varying from  $10^{-8}$  to  $10^0$ , while the order of magnitude of  $k_{MAPA}$  varies is from  $10^{-2}$  to  $10^0$ .

At low temperatures, the water term contribution is not very significant, especially at low concentrations. This is reflected in the linearity observed in the Arrhenius plots (Figure 6). For 3M and 4M the linear region goes up to 45°C, while at higher concentrations there's no linearity in the investigated temperature range.

This is due to a large contribution from the water term, as shown in Figure 7. These results are better analysed in Figure 7, which gives the contribution of the term for water as base, as defined by equation 24. For 5M the water term contribution is almost 90% at 60°C, and we can infer that at even higher temperatures and concentrations, the MAPA contribution would become negligible.

That the MAPA contribution becomes less important as its concentration increases may seem counterintuitive since the frequency of collisions between MAPA molecules would be expected to increase with concentration. This result could be only a numerical effect, due to the strong correlation between the regressed parameters, thus having no physical meaning. On the other hand, aqueous MAPA solutions are extremely non-ideal<sup>44</sup>, and the observed change in the behaviour of the contributions of MAPA and water to the kinetics may be a consequence of changes in the solution structure. Within the 1M to 5M MAPA concentration range, the activity of MAPA increases more than 10 times with increasing concentration<sup>44</sup>. This difference may be due to different orientations of MAPA molecules.

$$\%k_{H_2O} = \frac{a_{H_2O} \exp\left(\frac{b_{H_2O}}{T}\right) c_{H_2O} c_{MAPA}}{\left\{ a_{MAPA} \exp\left(\frac{b_{MAPA}}{T}\right) c_{MAPA} + a_{H_2O} \exp\left(\frac{b_{H_2O}}{T}\right) c_{H_2O} \right\} c_{MAPA}} \quad 24$$

The behaviour of the alpha parameters as functions of concentration of MAPA can be observed in

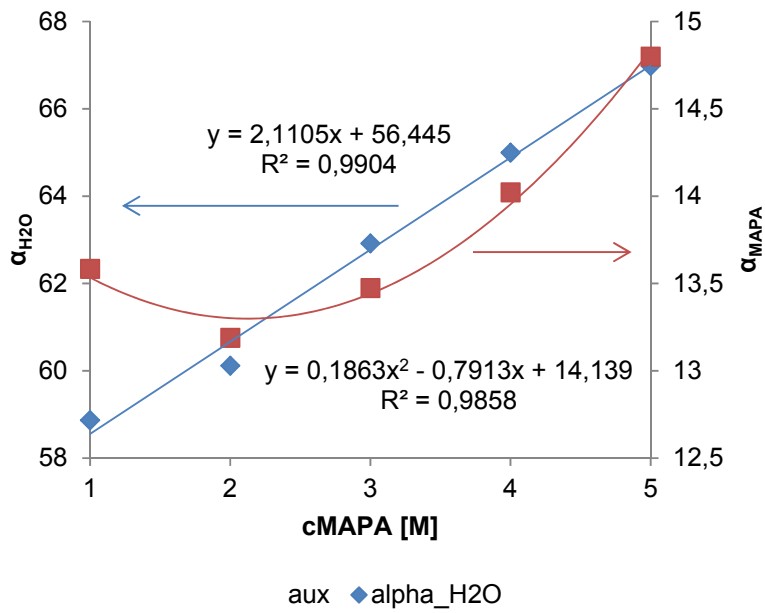


Figure 8. It is clear that the regressed  $\alpha_{H_2O}$  parameter increase almost linearly with concentration. It's value spans from 59 to 67, a change of 8 units that, transformed back to  $a_{H_2O}$ , means a change of 3 orders of magnitude. The regressed  $\alpha_{MAPA}$  parameters follow a second order polynomial with concentration. It's value spans from 13 to 15, a change of 2 units that, transformed back to  $a_{MAPA}$ , means a change of one order of magnitude.

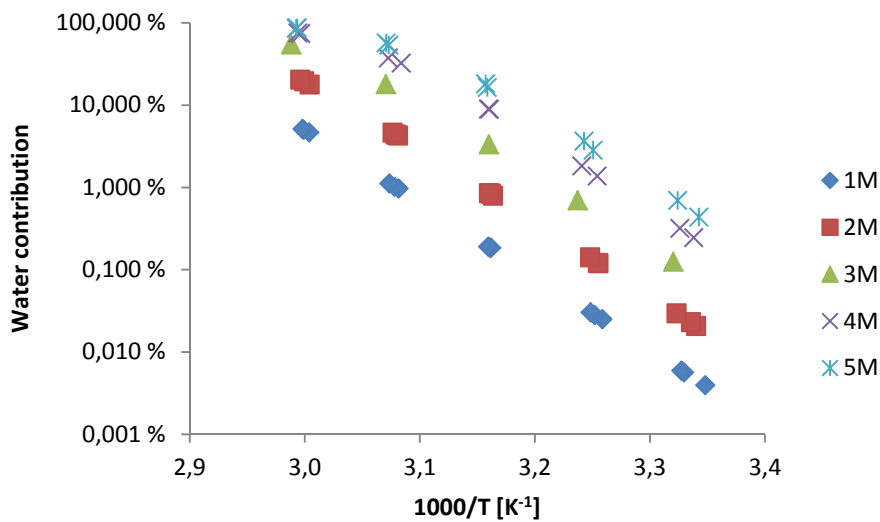
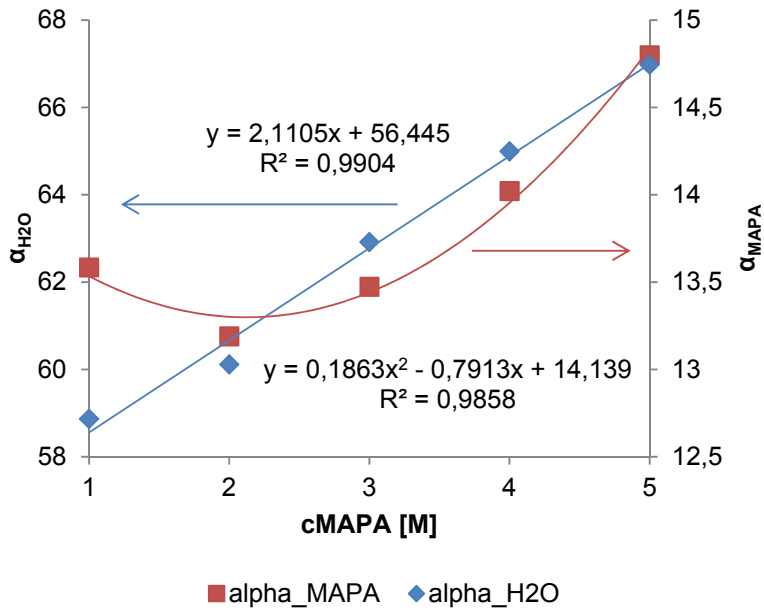


Figure 7 – Contribution of the water term, as defined by equation 24



**Figure 8 – Correlation for parameter values as functions of MAPA concentration**

In order to generalize the final correlation and since the regressed parameters were found to be highly correlated to the solution concentration, a new optimization was carried out, already incorporating the observed dependency when regressing the parameters. The expressions used for  $a_{MAPA}$  and  $a_{H_2O}$  are given in equations 25 and 26. The new objective function to be minimized is presented in equation 27. In this new formulation, a total of 7 parameters are regressed against all the experimental points available. The parameters are independent of both concentration and temperature. The optimum values are given in Table 5.

$$a_{MAPA} = \exp \left[ \beta_{MAPA} \left( \frac{c_{MAPA}}{1000} \right)^2 + \gamma_{MAPA} \frac{c_{MAPA}}{1000} + \theta_{MAPA} \right] \quad 25$$

$$a_{H_2O} = \exp \left( \gamma_{H_2O} \frac{c_{MAPA}}{1000} + \theta_{H_2O} \right) \quad 26$$

$$Fobj = \sum_{i=1}^{NP} \frac{\left\{ k_{obs}(i) - \left[ \exp \left[ \beta_{MAPA} \left( \frac{c_{MAPA}(i)}{1000} \right)^2 + \gamma_{MAPA} \frac{c_{MAPA}(i)}{1000} + \theta_{MAPA} + \frac{b_{MAPA}}{T} \right] c_{MAPA}(i) + \exp \left( \gamma_{H_2O} \frac{c_{MAPA}(i)}{1000} + \theta_{H_2O} + \frac{b_{H_2O}}{T} \right) c_{H_2O}(i) \right\}^2}{u_{kobs}^2(i)} \quad 27$$

**Table 5 – Parameters Regressed Using Equation 27**

Parameter	$\beta_{MAPA}$	$\gamma_{MAPA}$	$\theta_{MAPA}$	$b_{MAPA}$	$\gamma_{H_2O}$	$\theta_{H_2O}$	$b_{H_2O}$
Value	0.2092	-0.9437	12.5290	-4238.31	2.0041	64.9814	-24919.86

Attempts to simplify the expression in equation 25 by zeroing either  $\beta_{MAPA}$ ,  $\gamma_{MAPA}$  or both lead to large errors when predicting the observed kinetic constant. Using the expressions for  $a_{MAPA}$  and  $a_{H_2O}$  given in equations 25 and 26 leads to acceptable errors, but somewhat higher than those obtained previously, as seen when comparing the errors reported in Table 6 with those in Table 9 and as shown in Figure 5. This result is of great importance because equation 27 can be applied for any concentration and temperature within the experimental data range. This simplifies the implementation of rate based models in process simulators, for instance.

It should also be kept in mind that errors in  $k_{obs}$  will translate by their square root when back-calculated into transfer fluxes, i.e. 20% error in  $k_{obs}$  will give 10% error in mass transfer flux. The good agreement between the calculated and the experimentally determined CO<sub>2</sub> absorption fluxes can be observed in the parity plot presented in Figure 9, where all the points are between the y=0.9x and the y = 1.1x lines.



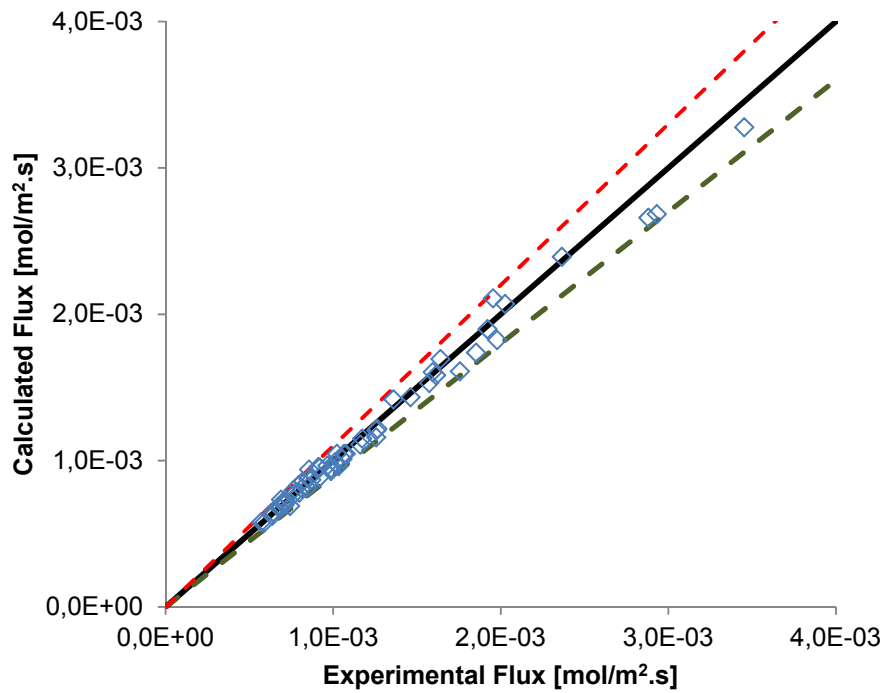


**Figure 9 – Parity plot for calculated vs. experimentally determined CO<sub>2</sub> absorption flux. Black line:  $y=x$ ; Red dashed line:  $y = 1.1x$ ; Green dashed line:  $y = 0.9x$ .**

**Table 6 – Optimization Results Using Equation 27**

MAPA concentration	Optimization using correlations	
	$F_{obj}$	ARD %
1M	7,2	8,5
2M	9,1	8,7
3M	2,1	8,7
4M	6,2	11,5
5M	24,2	34,2

Examples of joint confidence regions for the regressed parameters at a confidence level of 95% are given in Figure 10. During the optimization, the objective function was evaluated 600000 times (5000 iterations, swarm size = 40, operation repeated 3 times; for further information see Monteiro, Pinto, Zaidy, Hartono,

Svendsen <sup>43</sup>). The points that compose the joint confidence regions are those which fulfil the relationship presented in inequality 28. This inequality is exact for linear models only, but provide a very good approximation of the confidence regions for non-linear models <sup>41</sup>. It can be seen in Figure 10 that some parameters are strongly correlated to others. All the regressed parameters were found to be statistically significant.

$$F_{obj}(\underline{\Theta}) \leq F_{obj}(\hat{\underline{\Theta}}) \left( 1 + \frac{P}{NP-p} F_{p, NP-p}^{\sigma} \right) \quad 28$$

The values obtained for  $a_{MAPA}$  and  $b_{MAPA}$  are within the range of known kinetic constants for the carbamate reaction in alkanolamine solutions reported in literature <sup>13,45</sup>. Moreover, the  $k_{obs}$  value for MAPA has the same order of magnitude as the  $k_{obs}$  for piperazine (PZ) calculated from the data presented by Bishnoi, Rochelle <sup>32</sup>. A third diamine, AEEA 2-(2-aminoethyl-amino)ethanol, is found to have a performance closer to that of monoethanolamine (MEA) <sup>8</sup>. For comparison these values are presented in Table 7 for 1M solutions at 25°C.

**Table 7 –Kinetic Values Observed for Diamines and MEA, for 1M Solutions at 25°C**

Amine	$k_{obs}$ (s <sup>-1</sup> )	Source
MAPA	9.65E4	This work
PZ	5.37E4	Bishnoi and Rochelle (2000)
AEEA	1.21E4	Ma'mun et al. (2006)
MEA	6.00E3	Versteeg et al. (1996)

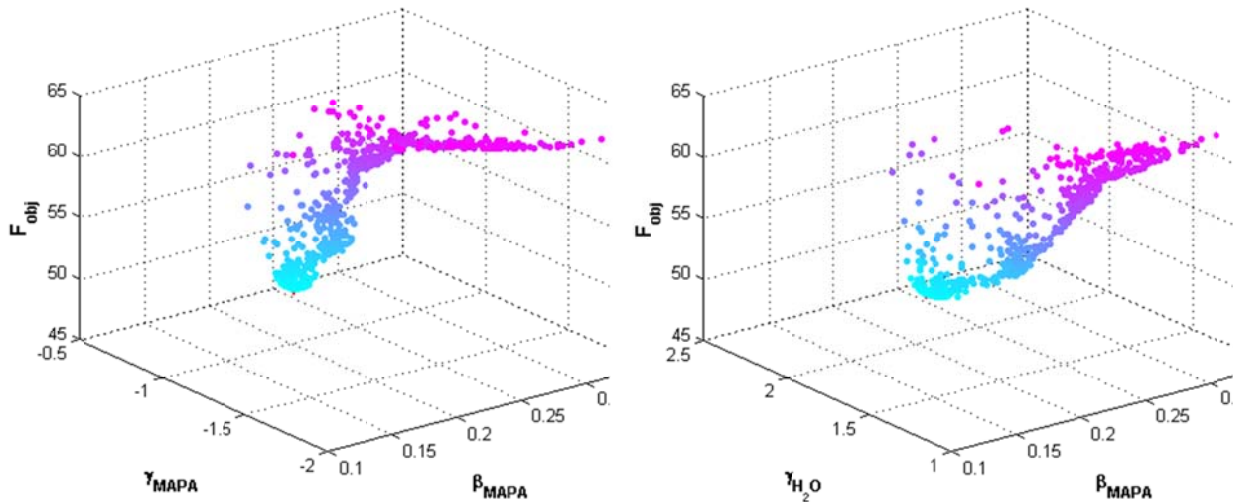


**Figure 10 – Example of joint confidence intervals for the estimated parameters.**

## Conclusions

The CO<sub>2</sub> absorption rate in unloaded MAPA aqueous solutions with concentrations varying between 1M and 5M were measured. The experimental temperature range was 25°C to 60°C. Because MAPA is a fast absorbing system, the CO<sub>2</sub> partial pressure was kept low, in the range of 0.1 to 0.3 kPa in the experiments performed in a string of discs contactor. Measurements for the 2M MAPA solutions were performed in a wetted wall column for pressures from 2kPa to 13kPa and the obtained overall mass transfer coefficients agree reasonably well with those obtained in the string of discs contactor.

All experiments were run on unloaded solutions. The reproducibility and repeatability of the experiments was found to be good. However, observed deviations between parallel evaluations of the overall mass transfer coefficient were around 5%, a value significantly larger than uncertainties calculated based on uncertainties in instrumental and analytical procedures (around 1%), but still very satisfactory.

To obtain values for the observed kinetic constant,  $k_{obs}$ , the experimental results were interpreted using a two-film mass-transfer model<sup>17</sup> and invoking the pseudo first order assumption. Needed experimental values for density, viscosity and Henry's law coefficient for CO<sub>2</sub> were measured and are given. The results indicate that MAPA is almost twice as fast as PZ, 8 times faster than AEEA, and 15 times faster than MEA, when comparing unloaded 1M solutions at 25°C.

The observed kinetic constant was modelled using the direct mechanism <sup>21</sup>, considering both water and MAPA as possible proton receivers. The observed kinetic constants of the model were unfolded using the Arrhenius representation, and the pre-exponential and energy parameters were regressed using the PSO algorithm <sup>40</sup>.

Very good agreement was obtained between the experimental data and the model, indicating that the direct mechanism can explain the MAPA carbamate formation reaction. However, the estimated pre-exponential parameter values for representing the reaction when water is the proton receiver were unreasonably high and a re-parameterization was applied to avoid numerical imprecisions which arise when computing large numbers.

The final expression for  $k_{obs}$  can be applied for any concentration and temperature within the experimental data range, and, together with the presented physical data, comprises a complete model for calculating absorption fluxes.

### Acknowledgments

Financial support from the EC 7th Framework Programme through Grant Agreement No : iCap-241391, is gratefully acknowledged

### Literature Cited

1. Chen X, Cloosmann F, Rochelle GT. Accurate screening of amines by the Wetted Wall Column. *Energy Procedia*. // 2011;4(0):101-108.
2. Brúder P, Svendsen HF. Capacity and Kinetics of Solvents for Post-Combustion CO<sub>2</sub> Capture. *Energy Procedia*. 2012;23(0):45-54.
3. Brúder P, Owrang F, Svendsen HF. Pilot study—CO<sub>2</sub> capture into aqueous solutions of 3-methylaminopropylamine (MAPA) activated dimethyl-monoethanolamine (DMMEA). *International Journal of Greenhouse Gas Control*. 11// 2012;11(0):98-109.
4. Liebenthal U, Pinto DDD, Monteiro JGM-S, Svendsen HF, Kather A. Overall Process Analysis and Optimisation for CO<sub>2</sub> Capture from Coal Fired Power Plants based on Phase Change Solvents Forming Two Liquid Phases. *Energy Procedia*. 2013;37:1844–1854.
5. Mangalapally HP, Notz R, Asprion N, Sieder G, Garcia H, Hasse H. Pilot plant study of four new solvents for post combustion carbon dioxide capture by reactive absorption and comparison to MEA. *International Journal of Greenhouse Gas Control*. 5// 2012;8(0):205-216.
6. Zhicheng X, Shujuan W, Bo Z, Changhe C. Study on potential biphasic solvents: Absorption capacity, CO<sub>2</sub> loading and reaction rate. *Energy Procedia*. // 2013;37(0):494-498.

7. Stephens EJ, Morris GA. Determination of Liquid-film Absorption Coefficients. *Chem. Eng. Progr.* 1951;47(5):11.
8. Ma'mun S, Dindore VY, Svendsen HF. Kinetics of the Reaction of Carbon Dioxide with Aqueous Solutions of 2-((2-Aminoethyl)amino)ethanol. *Industrial & Engineering Chemistry Research.* 2007/01/01 2006;46(2):385-394.
9. Knuutila H, Svendsen HF, Juliussen O. Kinetics of carbonate based CO<sub>2</sub> capture systems. *Energy Procedia.* // 2009;1(1):1011-1018.
10. Hartono A, Svendsen HF. Kinetics reaction of primary and secondary amine group in aqueous solution of diethylenetriamine (DETA) with carbon dioxide. *Energy Procedia.* 2009;1(1):853-859.
11. Luo X, Hartono A, Svendsen HF. Comparative kinetics of carbon dioxide absorption in unloaded aqueous monoethanolamine solutions using wetted wall and string of discs columns. *Chemical Engineering Science.* 9/12/ 2012;82(0):31-43.
12. Versteeg GF, van Swaaij WPM. Solubility and diffusivity of acid gases (carbon dioxide, nitrous oxide) in aqueous alkanolamine solutions. *J. Chem. Eng. Data.* // 1988;33(1):29-34.
13. Versteeg GF, Van Dijck LAJ, Van Swaaij WPM. On the kinetics between CO<sub>2</sub> and alkanolamines both in aqueous and non-aqueous solutions. An overview. *Chemical Engineering Communications.* 1996;144:113-158.
14. Hartono A, Mba EO, Svendsen HF. Physical properties of partially CO<sub>2</sub> loaded aqueous Monoethanolamine (MEA). *Submitted to Journal of Chem. & Eng. Data.* 2014.
15. Pinto DDD, Monteiro JGMS, Johnsen B, Svendsen HF, Knuutila H. Density measurements and modelling of loaded and unloaded aqueous solutions of MDEA (N-methyldiethanolamine), DMEA (N,N-dimethylethanolamine), DEEA (diethylethanolamine) and MAPA (N-methyl-1,3-diaminopropane). *International Journal of Greenhouse Gas Control.* 2014;25(0):173-185.
16. Knuutila H, Juliussen O, Svendsen HF. Density and N<sub>2</sub>O solubility of sodium and potassium carbonate solutions in the temperature range 25 to 80°C. *Chemical Engineering Science.* 3/15/ 2010;65(6):2177-2182.
17. Danckwerts PV. *Gas-liquid reactions.* New York: McGraw Hill; 1985.
18. Meyer VR. Measurement uncertainty. *Journal of Chromatography A.* 7/27/ 2007;1158(1-2):15-24.
19. Ciftja AF, Hartono A, Svendsen HF. Experimental study on phase change solvents in CO<sub>2</sub> capture by NMR spectroscopy. *Chemical Engineering Science.* 10/11/ 2013;102(0):378-386.
20. Danckwerts PV. The reaction of CO<sub>2</sub> with ethanolamines. *Chemical Engineering Science.* // 1979;34(4):443-446.
21. Crooks JE, Donnellan JP. Kinetics and mechanism of the reaction between carbon dioxide and amines in aqueous solution. *Journal of the Chemical Society, Perkin Transactions 2.* 1989;0(4):331-333.
22. da Silva EF, Svendsen HF. Ab Initio Study of the Reaction of Carbamate Formation from CO<sub>2</sub> and Alkanolamines. *Ind. Eng. Chem. Res.* // 2004;43(13):3413-3418.
23. Shim J-G, Kim J-H, Jhon YH, Kim J, Cho K-H. DFT Calculations on the Role of Base in the Reaction between CO<sub>2</sub> and Monoethanolamine. *Industrial & Engineering Chemistry Research.* 2009/02/18 2009;48(4):2172-2178.
24. Arstad B, Blom R, Swang O. CO<sub>2</sub> Absorption in Aqueous Solutions of Alkanolamines: Mechanistic Insight from Quantum Chemical Calculations. *The Journal of Physical Chemistry A.* 2007/02/01 2007;111(7):1222-1228.
25. Gibson KD. True and apparent activation energies of enzymic reactions. *Biochimica et biophysica acta.* Feb 1953;10(2):221-229.

26. Schwaab M, Pinto JC. Optimum reference temperature for reparameterization of the Arrhenius equation. Part 1: Problems involving one kinetic constant. *Chemical Engineering Science*. 5// 2007;62(10):2750-2764.
27. da Silva EF, Kuznetsova T, Kvamme B, Merz KM. Molecular Dynamics Study of Ethanolamine as a Pure Liquid and in Aqueous Solution. *The Journal of Physical Chemistry B*. 2007/04/01 2007;111(14):3695-3703.
28. Han B, Zhou C, Wu J, Tempel DJ, Cheng H. Understanding CO<sub>2</sub> Capture Mechanisms in Aqueous Monoethanolamine via First Principles Simulations. *The Journal of Physical Chemistry Letters*. 2011/03/17 2011;2(6):522-526.
29. Han B, Sun Y, Fan M, Cheng H. On the CO<sub>2</sub> Capture in Water-Free Monoethanolamine Solution: An ab Initio Molecular Dynamics Study. *The Journal of Physical Chemistry B*. 2013/05/16 2013;117(19):5971-5977.
30. Gupta M, da Silva EF, Svendsen HF. Carbamate Stability Constants of Amines and their Temperature Dependency using Explicit Solvation Shell Model and Continuum Solvation Models. *Submitted to Journal of Physical Chemistry B*. 2014.
31. Hartono A, da Silva EF, Svendsen HF. Kinetics of carbon dioxide absorption in aqueous solution of diethylenetriamine (DETA). *Chemical Engineering Science*. 7/15/ 2009;64(14):3205-3213.
32. Bishnoi S, Rochelle GT. Absorption of carbon dioxide into aqueous piperazine: reaction kinetics, mass transfer and solubility. *Chemical Engineering Science*. 11// 2000;55(22):5531-5543.
33. Kim I. *Heat of reaction and VLE of post combustion CO<sub>2</sub> absorbents*. Trondheim, Norway: PhD Thesis. Faculty of Natural Sciences and Technology, Department of Chemical Engineering, Norwegian University of Science and Technology, NTNU; 2009.
34. Levenspiel O. *Chemical Reaction Engineering* (3rd Edition): John Wiley & Sons; 1999.
35. Brauner N, Shacham M. Statistical analysis of linear and nonlinear correlation of the Arrhenius equation constants. *Chemical Engineering and Processing: Process Intensification*. 6// 1997;36(3):243-249.
36. Curl RL. Letters to the editor. *AIChE Journal*. 1993;39(8):1420-1420.
37. Sundberg R. Statistical aspects on fitting the Arrhenius equation. *Chemometrics and Intelligent Laboratory Systems*. // 1998;41(2):249-252.
38. Chen NH, Aris R. Determination of Arrhenius constants by linear and nonlinear fitting. *AIChE Journal*. 1992;38(4):626-628.
39. Klicka R, Kubáček L. Statistical properties of linearization of the Arrhenius equation via the logarithmic transformation. *Chemometrics and Intelligent Laboratory Systems*. 11// 1997;39(1):69-75.
40. Kennedy J, Eberhart R. Particle swarm optimization. Paper presented at: Neural Networks, 1995. Proceedings., IEEE International Conference on; Nov/Dec 1995, 1995.
41. Schwaab M, Biscaia JEC, Monteiro JL, Pinto JC. Nonlinear parameter estimation through particle swarm optimization. *Chemical Engineering Science*. 3// 2008;63(6):1542-1552.
42. Poli R, Kennedy J, Blackwell T. Particle swarm optimization. *Swarm Intell*. 2007/06/01 2007;1(1):33-57.
43. Monteiro JGMS, Pinto DDD, Zaidy SAH, Hartono A, Svendsen HF. VLE data and modelling of aqueous N,N-diethylethanolamine (DEEA) solutions. *International Journal of Greenhouse Gas Control*. 11// 2013;19(0):432-440.
44. Hartono A, Saleem F, Arshad MW, Usman M, Svendsen HF. Binary and ternary VLE of the 2-(diethylamino)-ethanol (DEEA)/3-(methylamino)-propylamine (MAPA)/water system. *Chemical Engineering Science*. 9/20/ 2013;101(0):401-411.
45. Vaidya PD, Kenig EY. CO<sub>2</sub>-Alkanolamine Reaction Kinetics: A Review of Recent Studies. *Chemical Engineering & Technology*. 2007;30(11):1467-1474.

